JOURNAL OF MATERIALS SCIENCE **38** (2003) 3755–3763

Defect depth profiling after sphere indentation and blasting in aluminum and aluminum alloy detected by positron annihilation

EWA DRYZEK
H. Niewodniczański Institute of Nuclear Physics, ul. Radzikowskiego 152, 31-342 Kraków, Poland
E-mail: ewa.dryzek@ifj.edu.pl

The paper presents the experimental results of positron annihilation measurements of the subsurface zones in aluminum and aluminum alloy exposed to the indentation of the small steel ball or blasting by the silicon carbide particles. The measurements of the Doppler broadening of the annihilation line and positron lifetime (PL) enabled the depth profile of open volume defects induced by indentation and blasting processes to be obtained. The coincidence of the von Mises criterion for yield with the onset of the increase of the defect concentration at certain depth was detected. It was established that the defects created in the pure aluminum and the aluminum alloy detected by positrons are different. However, the kinds of induced defects do not change with depth. The PL measurements indicate the presence of vacancy clusters in samples exposed to blasting. The vacancy clusters created in the aluminum alloy are larger than in the pure aluminum.

1. Introduction

The elastic stress fields generated by an indenter in a flat extensive specimen are complex but well-defined. However in ductile materials blunt indenter such as a sphere or cylindrical punch may readily induce plasticity [1]. When the response of the specimen material is elastic-plastic theoretical treatments are limited by simplifying assumptions [2]. Generally, the results of theoretical calculations of the stress fields e.g., based on the finite element method, are compared with experimentally observed phenomena (e.g. [3]). Optical microscopy, scanning and transmission electron microscopy and X-ray diffraction are among the standard methods extensively used for characterization of subsurface deformation.

Application of positron annihilation spectroscopy may give the complementary information on microstructure of the deformed subsurface region. This method is used in studies of crystal lattice defects in metals and alloys. It is specifically sensitive to open volume defects such as vacancies, vacancy clusters, microvoids or dislocations. When a positron enters the sample, its kinetic energy becomes equal to the thermal energy very rapidly. After reaching the thermal energy the positron diffusing in a crystal lattice samples about 10^6 lattice sites. Then the positron annihilates with an electron with release of a γ-quantum pair. It is well established that the emitted γ quanta reflect the local microscopic electronic properties since the positron energy is negligible in comparison with the electron energy. Positrons diffusing in the crystal lattice are strongly attracted by open volume defects, like vacancies, vacancy clusters or voids. The trapping of positrons into these defects causes the changes in the measured positron annihilation characteristics such as: the positron lifetime, the energy spectrum (the Doppler broadening of the annihilation line) and the angular correlation of the annihilation quanta. The sensitivity of the positron lifetime spectroscopy to the open volume defects is based on the fact that the positron annihilation rate is determined by the electron density in the defect. Positron lifetime spectrum consists of one or more components in the form of exponential decay lines described by their decay rates λ_i and intensities I_i. The positron lifetime $\tau_i = 1/\lambda_i$. If the volume of the defect the positron is trapped in increases the value of the positron lifetime also increases.

Positron annihilation method allows detecting a minimum vacancy concentration of an order of 0.1 ppm. Other defects created by plastic deformation such as dislocations are capable of trapping positrons due to their localization by e.g., jogs at the dislocation line [4]. Positron annihilation method is not sensitive to interstitial atoms.

Positron annihilation techniques have been applied to study defects induced by e.g., plastic deformation, thermal generation of vacancies or radiation damage. Application in deformed materials has been reported in the literature e.g. [5–7].

Our previous works [8–10] concerned the positron annihilation study of the subsurface zones in copper arising as an effect of different processes like

indentation, compression, blasting but also sliding friction: dry and with lubrication. In case of indentation we found that the defect depth distribution exhibited a complex structure as indicated by the presence of layers with different defect concentrations. The defect depth distribution produced in the blasting process of copper samples had different character and was similar to that obtained as a result of sliding of a steel ball on a copper surface [9, 10]. Considering the widespread applications of aluminum and aluminum alloys it is interesting to investigate the defect depth distribution in these materials. Comparison of the obtained results with the results for copper would be interesting on account of the difference in the stacking fault energy (SFE) which is known to have strong impact on the microstructure of the deformed metal. Aluminum is an example of a high SFE while the value of SFE for copper is intermediate between high and low SFE materials.

In the present work positrons were used for probing the aluminum and aluminum alloy samples after plastic deformation by a load indenter or after blasting with silicon carbide particles. The first case corresponds to deformation at a low strain-rate as the indenter penetrates into the material, in the latter the strain-rates in the surface layer are much higher. The results of the positron annihilation measurements were compared with the results of theoretical calculations of the stress fields obtained with the elastic theory.

2. Experimental details

2.1. Sample preparation

We used well annealed 99.999% purity Al samples in the shape of discs 25 mm in diameter 4 mm thick and 6082-T6 (AlMgSi1Mn) aluminum alloy samples in the form of plates 15 mm × 15 mm × 10 mm cut from a sheet. The chemical composition of the alloy was: 97.4 wt% of Al, 0.9 wt% of Mg, 0.7 wt% of Mn, 1 wt% of Si.

The Al samples were annealed in vacuum at 600°C for 1 h and then cooled within the furnace to room temperature. No thermal treatment was performed for the aluminum alloy samples.

On the surface of the samples indentations were made in 1 mm distance in two perpendicular directions covering an area of 15 mm × 15 mm. This was necessary because the diameter of the ^{22}Na source (activity 40 μCi) emitting positrons was 10 mm. The indenter was a martensite steel ball 4 mm in diameter and the indentations were made in same way as in the Rockwell hardness test. The loads applied to the indenter were equal to 10 N and 20 N.

The traces of indentations on the sample surface had the shape of circles whose diameters, as measured with a metallographic optical microscope, were equal to 0.75 mm for the load of 20 N and 0.59 mm for the load 10 N for the aluminum. The ratio of the treated area to the whole area covered by the source was 44% and 27%, respectively. The diameters of indentations in aluminum alloy were equal to 0.35 mm for the load of 20 N and 0.29 mm for the load of 10 N. The ratio of the treated area to the whole area covered by the source was 10% and 5%, respectively.

In each case two identical samples were prepared and the source, enveloped in the kapton foil 7 μm thick, was sandwiched between them. After the positron annihilation measurement samples were etched to remove a layer of thickness of about 30 μm from the surface and the next measurement was performed. The solution for aluminum etching was as follows: 30 g NaCl, 200 g NaOH, 1 litre of distilled water. The solution for aluminum alloy etching was slightly different: 50 g NaOH, 40 g NaF, 0.91 litre distilled water. In both cases etching was carried out at 50°C.

Additionally samples of aluminum and aluminum alloys were prepared whose surfaces were blasted by silicon carbide particles with an air pressure 6.5 bar. The silicon carbide particles had diameter less than 0.5 mm and an irregular shape with sharp edges. The procedure of sequenced measurements described above was applied also to the blasted specimens. Both surface treatments of samples: the indentations and blasting were performed at room temperature.

2.2. The positron annihilation measurements

The Doppler broadening of the annihilation line was used in our investigations. In this method the energy spectrum of the annihilation radiation is usually measured with a high-purity germanium detector. The obtained spectrum is characterized by the so-called shape parameters [11]. The S-parameter the one that is the most frequently used. It is defined as the ratio of the area under the fixed central part of the annihilation line to the area under the whole annihilation line. It is sensitive to the annihilation of positrons with low momentum electrons which are present in open volume defects. The electrons in the interstitial regions of the perfect lattice have slightly higher momenta. Then the S-parameter is sensitive to the average density of open volume defects. Similarly one can define the W-parameter as the ratio of the area under the fixed wing region of the annihilation line to the area under the whole annihilation line. This region reflects the annihilation with high momentum electrons. A change of the slope of the S-W dependence indicates a change of the defect type in the material.

The Doppler broadening of the annihilation line was measured using the spectrometer with the high-purity germanium detector (HpGe) with energy resolution FWHM = 1.40 keV at 586 keV. There were extracted from the spectrum the shape parameters. The energy range for calculation of the S-parameter was (511 ± 1.13) keV and for W-parameter (516.41–516.94) keV.

The sequenced measurements enabled to obtain the S-parameter depth profile which is a convolution of the positron implantation profile and the actual S-parameter depth profile. Fast positrons emitted from the radioactive source ^{22}Na are implanted at the depth of a few tens of micrometers depending on the material of the specimen. In the case of aluminum 84.7% of positrons are stopped to the depth 94 μm [12]. In one measurement the contribution to the obtained value of

the S-parameter originates from the some depth range. The depth resolution of the method in case of aluminum seems to be much lower then in the case of copper for which the corresponding value is equal to 28 μm. Nevertheless, if the defect profile extends up to a few hundreds of micrometers the changes of the S-parameter with the depth are visible. At this stage it is difficult to deconvolute obtained experimental dependencies. However, for example the measured exponential decay of the S-parameter reproduces the exponential decay of the defect concentration and the presence of the layer with higher defect concentration than the surrounding regions causes the rise of the S-parameter value [13]. Comparatively high penetration depth of the positrons from the ^{22}Na radioactive source in aluminum causes smoothing of the S-parameter changes.

Additional positron lifetime measurements were performed using a conventional *fast-fast* coincidence lifetime spectrometer with BaF_2 scintillators with the time resolution (FWHM) of 240 ps for the ^{22}Na energy window. Data were analyzed using the LT version 2.5 computer program [14]. In the analysis of the PL spectra, the background and source corrections were taken into account.

Positron annihilation measurements were performed at room temperature.

3. Experimental results

3.1. Expected positron trapping defects and the influence of sample preparation

It is well known that in a plastically deformed metal dislocations are created. Moving dislocations with jogs produce tracks of point defects. After a deformation the sample contains dislocations and a higher than equilibrium concentration of vacancies and interstitials. The high mobility of interstitial in aluminum causes their annihilation at temperatures higher than 50 K [15]. The migration of vacancies takes place below 0°C [16]. After a deformation at room temperature it is expected that the aluminum samples contain a high dislocation density and vacancy loops or small vacancy clusters produced by agglomeration of vacancies [17]. Increase of the S-parameter value after deformation in comparison with the value for the well-annealed sample indicates the presence of defects trapping positrons.

To exclude the influence of the etching temperature on the sample the rolled Al (99.999%) specimens were kept in water at 50°C for 15 min. The S-parameter values did not change within experimental error. The fact that influence of etching at 50°C on the defect structure is small seems to be confirmed by the experimental results of the S-parameter measurements for isochronal annealing of the single crystal aluminum specimens strained by rolling at room temperature reported in [17]. The temperature at which the S-parameter starts decreasing depends on the degree of deformation and for 48% deformation takes place at 90°C. For smaller deformations the reduction of the S-parameter to the reference value takes place at higher temperatures. For the temperature range between room temperature and 50°C changes of the S-parameter are small.

It seems that the hydrogen uptake during etching is negligible. After taking off a few layers from the pure aluminum sample surface, the S-parameter approached to the value measured for the untreated well-annealed sample. For the aluminum alloy the hydrogen solubility should be comparable.

3.2. Aluminum

3.2.1. Indentation treatment

Figs 1 and 2 present the depth profiles of the S-parameter for the aluminum samples exposed to an indentation test with normal loads of 10 N and 20 N, respectively. The dashed horizontal line marks the value of the S-parameter for the non-damaged surface which corresponds to the bulk value characteristic for the material without open volume defects induced by deformation. On the right side of each figure the appropriate S-W plot is presented.

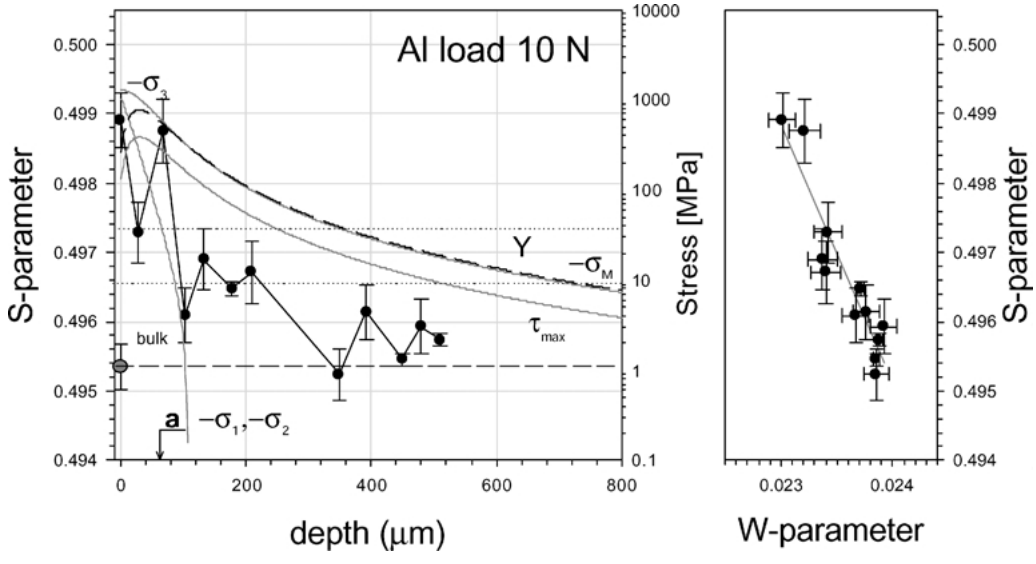

Figure 1 S-parameter depth-profile for the high purity aluminum sample (closed circles) whose surface was covered by indentations with a steel ball under a normal load of 10 N. The solid lines present the calculated principal stresses beneath the ball. The dashed line presents the σ_M resulting profile of the von Mises stress and **a** marks the Hertz radius given by equation (1). The right part of the figure presents the S-W plot.

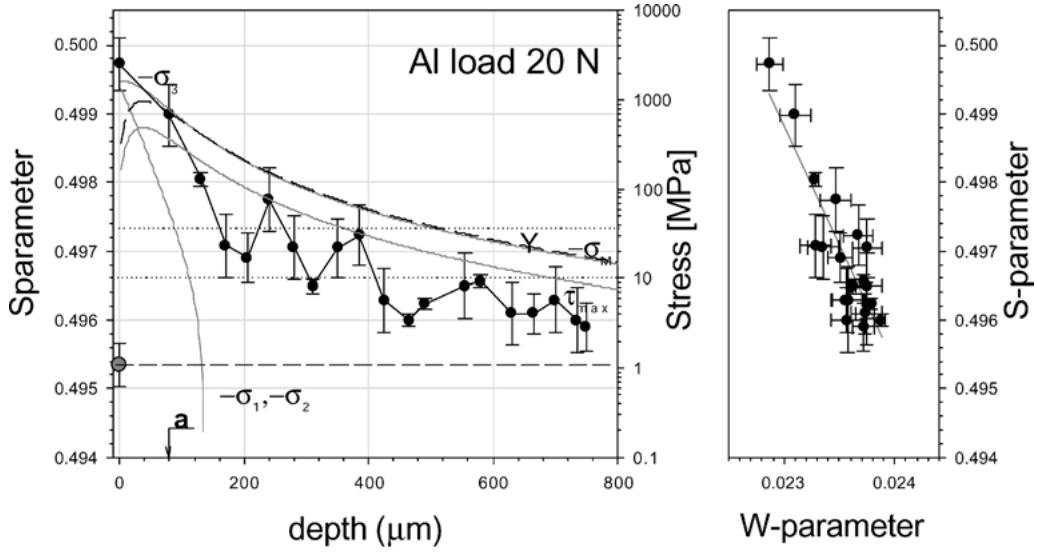

Figure 2 S-parameter depth-profile for the high purity aluminum sample (closed circles) which surface was covered by indentations with a steel ball under a normal load of 20 N. The solid lines present the calculated principal stresses beneath the ball. The long dashed line presents the σ_{M} resulting profile of the von Mises stress and **a** marks the Hertz radius given by equation (1). The right part of the figure presents the S-W plot.

The value of the S-parameter for the surface is higher for the higher load, i.e., 20 N. Also the depth at which the S-parameter approaches to the bulk value depends on the load. For 10 N it is about 400 μm and for 20 N it is above 700 μm. For both loads the dependences of the S-parameter on the depth are not smooth.

For a load of 10 N the fluctuations are biggest in the range of first 120 μm and the drop of the S-parameter value at this depth is significant. Then the decrease of the S-parameter with increasing depth is slower. Similarly for a load of 20 N the drop of the S-parameter value is biggest in the range of first 160 μm. In the following depth range the S-parameter exhibits some maxima: at 220 μm, 390 μm and 480 μm. These may reflect the presence of layers with different defect concentrations. In this case the maxima correspond to layers with higher defect concentration than in the neighboring area. For 10 N the area between 140 μm and 210 μm with higher values of the S-parameter may be distinguished. However, the confirmation of the presence of the layers with different defect concentrations requires further measurements.

The slopes of the straight lines fitted to the experimental points in the W-S plots do not differ significantly: -3.72 ± 0.44 for 10 N and -3.49 ± 0.42 for 20 N.

In Figs 1 and 2 we plot as well the principal stresses distribution, σ_{1-3}, direct beneath the spherical indenter according to the relations published in [1] and obtained by Huber [18] (see Appendix). Along the z axis at $r = 0$ the two principal stresses are equal $\sigma_2 = \sigma_1$ Taken with the negative sign they are smooth rapidly decreasing functions of the depth. The value of $-\sigma_3$ also decreases but it changes more slowly with the depth. The function $\sigma_{\mathrm{M}} = \sqrt{\frac{1}{2}[(\sigma_1 - \sigma_2)^2 + (\sigma_2 - \sigma_3)^2 + (\sigma_3 - \sigma_1)^2]}$ used in the von Mises criterion for yield is also plotted. The dotted horizontal lines present the range of the yield stress values given by the aluminum supplier, (10–35) MPa [19]. Below the depth at which the von Mises criterion is fulfilled i.e., $\sigma_{\mathrm{M}} = Y$ the S parameter reaches the bulk value for the load 10 N. For the load 20 N the S-parameter value also diminishes significantly. It means that no plastic deformation occurred deeper. We observed a similar effect for copper [8]. It is difficult to find other coincidences between the measured S-parameter depth profile and the calculated elastic indentation stress fields, solid lines in Figs 1 and 2.

In the literature one can find so-called expanding cavity model proposed by Johnson [20] (see also [1]) which describes the plastic deformation beneath a ball indenter. Plastic deformation in the vicinity of the indenter is compared to that which occurs during the radial expansion of a spherical cavity subjected to internal pressure. Johnson replaced the expanding spherical cavity with an incompressible, hemispherical core of material directly beneath the indenter of radius equal to the contact circle, a. The core hemisphere is surrounded by a hemispherical plastic zone which connects with the elastically strained material at some radius. The radius of the contact circle and core hemisphere one can calculate using the Hertz radius:

$$a = \sqrt[3]{\frac{4}{3}\frac{k\,P\,R}{E}}, \tag{1}$$

where P is the normal load, R is the radius of the ball, and k is the elastic mismatch parameter given by $k = 9[(1 - \nu^2) + E(1 - \nu'^2)/E']/16$. Here, E' and ν' are the Young's modulus, the Poisson's ratio of indenter material, respectively. The radius of the plastic hemisphere can be estimated from the von Mises criterion mentioned above. In Figs 1 and 2 we marked the radius a. Note the distinct drop of the S-parameter in the vicinity of the radius $a$value which could mark the border between the core and the plastic hemisphere. This can support the expanding cavity model. Nevertheless, such a behavior at the Hertz radius was not observed for copper [8].

3.2.2. Blasting treatment

Fig. 3 presents the dependence of the S-parameter on the depth for the aluminum sample blasted by the silicon carbide particles at a pressure of 6.5 bar. The value of the S-parameter for the surface is higher then for samples exposed to indentations. The S-parameter even increases at depth 30 μm, then decreases smoothly and eaches the bulk value at the depth 300 μm. Passing over the value of the S-parameter for the surface, the exponential decay function:

$$S(z) = S_0 + A \exp\left(-\frac{z}{d_0}\right) \tag{2}$$

can be fitted to the remaining experimental points. The obtained values of parameters are following: $S_0 = 0.4947 \pm 0.0004$, $A = 0.0118 \pm 0.0006$, $d_0 = (115 \pm 15)$ μm.

The slope of the W-S plot equals –4.50 ± 0.44 and differs slightly from the values for other aluminum samples.

3.3. Aluminum alloy

3.3.1. Indentation treatment

The results obtained for the aluminum alloy samples exposed to indentations with loads of 10 N and 20 N are presented in the Figs 4 and 5, respectively. The aluminum alloy samples were made of raw material, which contained defects associated with structure and/or induced by mechanical working. In spite of the lack of earlier annealing the indentation, especially with the higher load, produces additional defects. This is

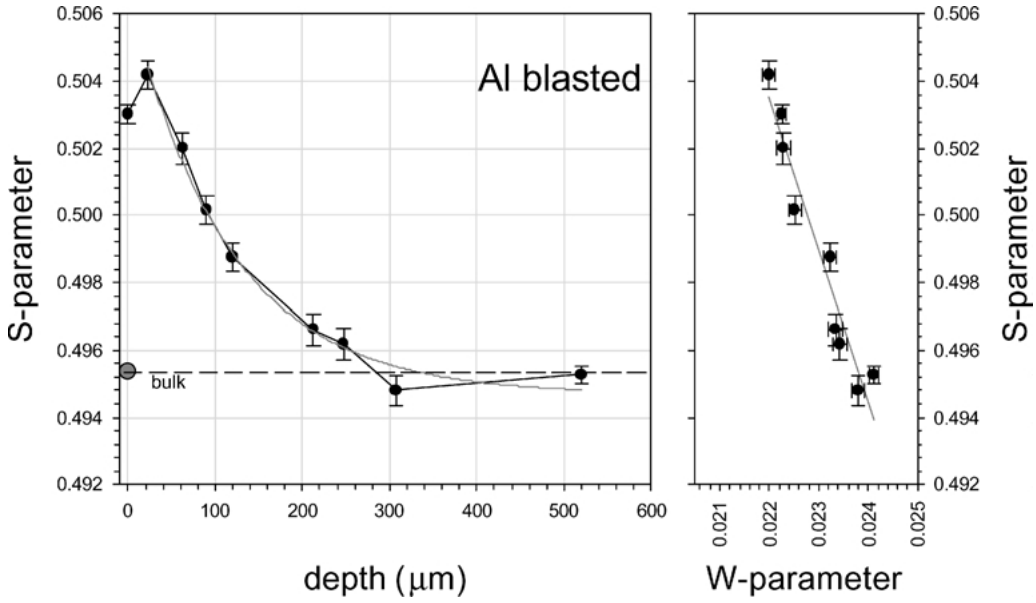

Figure 3 S-parameter depth-profile for a high purity aluminum sample after blasting with small silicon carbide particles with a pressure of 6.5 bar. The solid curve presents the best fit of the relation (2) to the experimental points except the point at the surface. The right part of the figure presents the S-W plot.

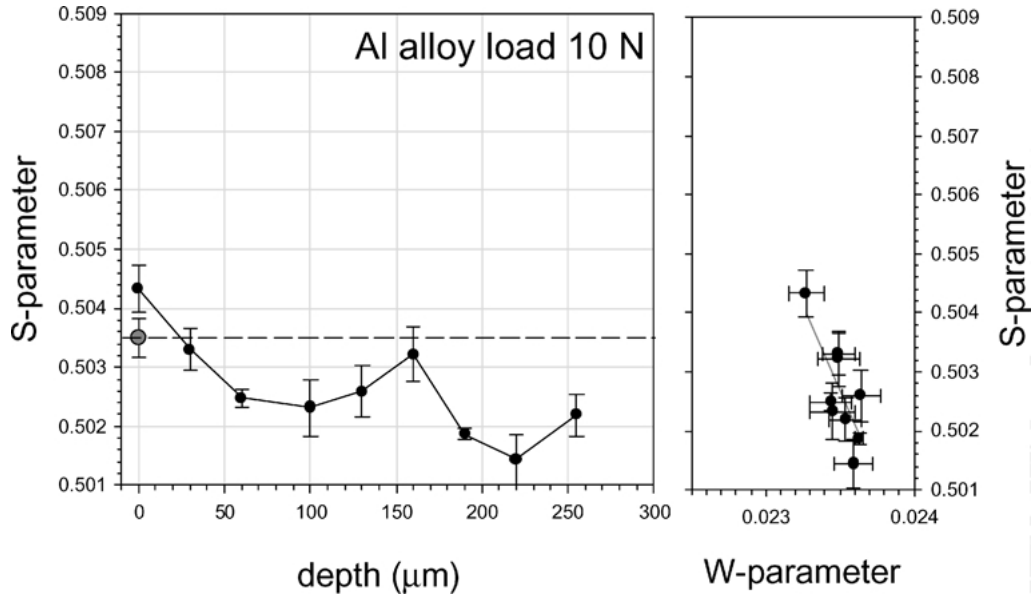

Figure 4 S-parameter depth-profile for the aluminum alloy sample (closed circles) which surface was covered by indentations with a steel ball under a normal load of 10 N. The right part of the figure presents the S-W plot.

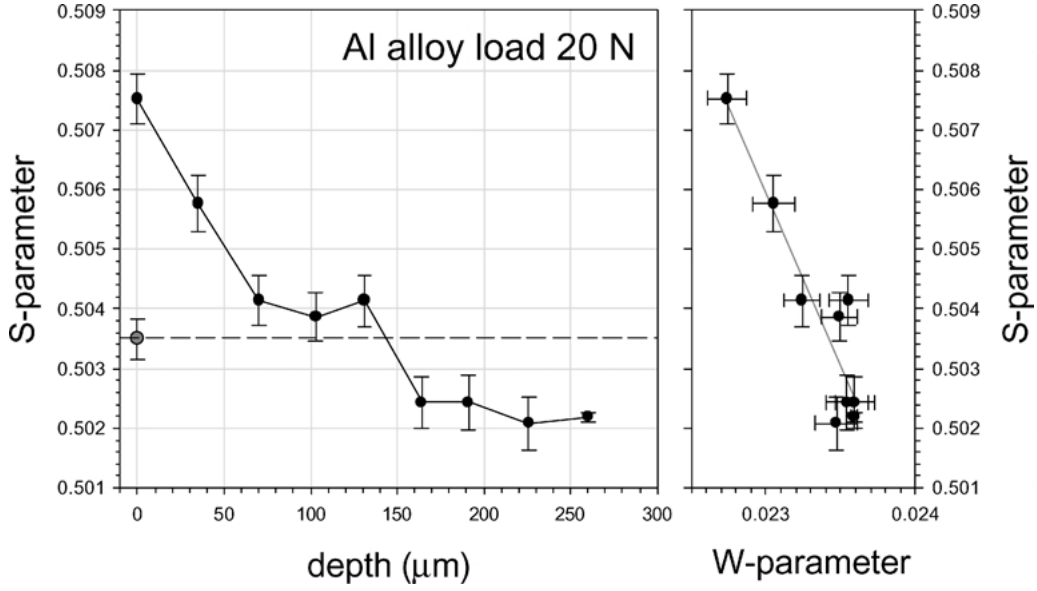

Figure 5 S-parameter depth-profile for the aluminum alloy sample (closed circles) which surface was covered by indentations with a steel ball under a normal load of 20 N. The right part of the figure presents the S-W plot.

reflected in the rise of the S-parameter value, Figs 4 and 5. For the load 10 N the increase of the surface value of the S-parameter is small. Then the S-parameter decreases below the surface value for the untreated sample and exhibits a maximum at 160 μm. The maximum may signify the layer with higher concentration of defects. For the sample exposed to the indentation with the load 20 N, starting from the surface the S-parameter decreases to the depth 60 μm getting the almost constant value at the depth range 60 μm–130 μm which is little bit higher than the surface value of the S-parameter for the sample before treatment, Fig. 5. This may be connected with the presence of a layer with higher concentration of defects as in the case of the load 10 N. Then the S-parameter decreases to the lower value. The total range of the S-parameter change ends at the depth 160 μm, which is considerably less than for the aluminum sample. The fact that the S-parameter in both cases decreases to a value lower than the surface value for untreated sample indicates that concentration of defects in the surface layer of the untreated sample is higher than in the deeper layers. This is a consequence of the mechanical treatment of the raw material and lack of annealing. The slopes of the straight lines fitted to the experimental points in the W-S plots are equal -5.78 ± 1.83 and -5.73 ± 0.93 for loads 10 N and 20 N, respectively.

3.3.2. Blasting treatment

Fig. 6 presents the dependence of the S-parameter on the depth for the blasted sample of aluminum alloy. The total depth range of the S-parameter changes, ca. 300 μm, is much bigger then for the aluminum alloy samples exposed to indentations but surprisingly it is comparable to total depth range for the blasted

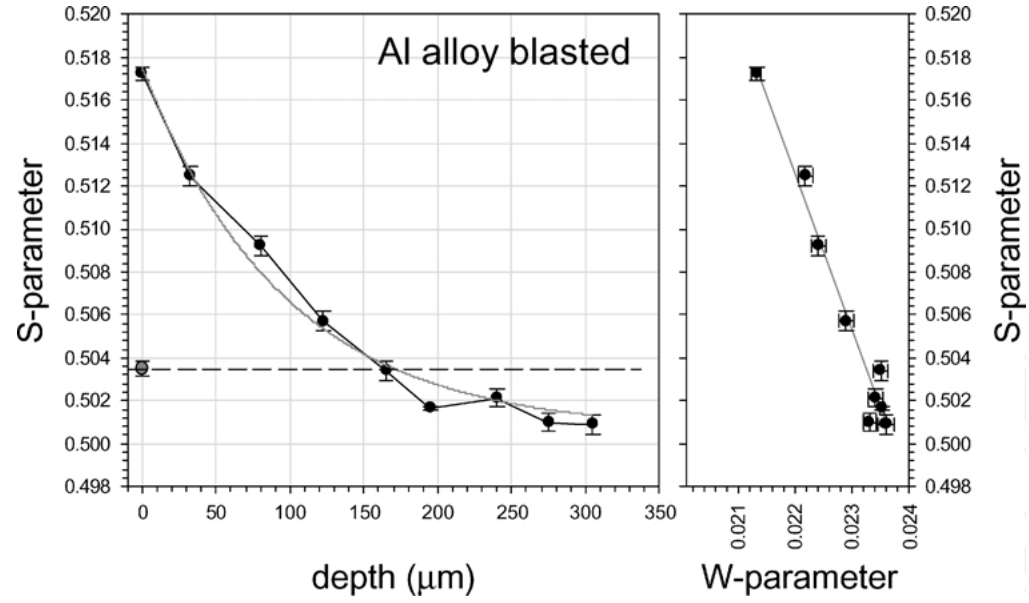

Figure 6 S-parameter depth-profile for the aluminum alloy sample after blasting with small silicon carbide particles with a pressure of 6.5 bar. The solid curve presets the best fit of the relation (2) to the experimental points. The right part of the figure presents the S-W plot.

pure aluminum sample. The parameter d_0 obtained from the fitting of the relation (2) to the experimental points is also similar: $d_0 = (120 \pm 15)\ \mu$m. Remaining parameters are following: $S_0 = 0.4990 \pm 0.0008$ and $A = 0.0182 \pm 0.0008$. However, in this case a layer at the surface with lower concentration of defects is not present. The slope of the fitted straight line in the W-S plot is -7.30 ± 0.52.

4. Discussion

4.1. Aluminum

As was mentioned previously the deformed samples contained a high number of dislocations and vacancy loops or small vacancy clusters. The results of the theoretical calculations of positron states [21] showed that dislocations in aluminum are very shallow traps but vacancies and single jogs at the dislocation line can localize positrons which result with a lifetime of about 224 ps. It is in a good agreement with the experimentally observed lifetimes in aluminum containing dislocations (228 ± 1 ps) see e.g., [22]. The experimental value of the positron lifetime for the bulk vacancy is between 244 ps and 251 ps [23–25] (the calculated value is 254 ps [21]). The calculated lifetimes for vacancy clusters given in [26] are higher. The experimental value of the bulk positron lifetime for aluminum is 163 ps–166 ps [23, 25, 27]. In the case of the Doppler broadening measurements positrons annihilating trapped in the different kind of open volume defects contribute to the rise of the S-parameter. The one straight line fitted to the W-S dependency suggests that the type of defects trapping positrons does not change with the depth, but its concentration decreases with increasing depth. The single straight lines were fitted to the experimental points plotted in the W-S graphs for the aluminum exposed to indentations (Figs 1 and 2) although in the region where the S-parameter approaches to the bulk value the departures of the points from the straight line could suggest the possibility of fitting of the another straight line with a different slope. This could be connected with a change of the type of the positron trapping sites at the depth in the vicinity of the bulk material but such a conclusion could not be justified because the changes of the W- and S-parameter in this region are small in comparison with the whole range of these parameter changes.

The average slopes of the straight lines fitted to the experimental points in the W-S plots for the indentation of the aluminum samples with the loads of 10 N (-3.72 ± 0.44) and 20 N (-3.49 ± 0.42) do not differ within experimental error. This indicates that for both loads the defects generated in the material are of the same type.

For the blasted aluminum sample the dependence of the S-parameter on the W-parameter suggest that the type of created defects also does not change in the whole depth range but the slope of the straight line has the lower value than for the samples exposed to indentations, which indicates different type of positron trapping sites. In order to learn more about the type of defects present in the samples the positron lifetime measurements were performed. Results of such measurements not always are sufficiently accurate to decide whether the lifetime spectra contain one or two components as it was reported by Petersen in the case of the aluminum single-crystal deformed 50% by rolling [17]. In such a case only the mean positron lifetime may be considered. Electron microscopy revealed the presence of vacancy loops with a size distribution. In our case the deconvolution of positron lifetime spectrum into two components was made. The first component coming from the bulk was equal to (151 ± 7) ps and the second equal to (272 ± 8) ps with the intensity (43.4 ± 3.5) may correspond to the annihilation of positrons trapped at clusters of two vacancies [26]. The mean lifetime $\bar{\tau}$ was equal to 204 ps.

Exponential decay of the S-parameter depth profile for the blasted aluminum indicates that the defect concentration also decreases exponentially with the increasing depth [12]. Similar exponential decay was observed for the blasted copper but without the initial increase of the S-parameter. This increase may be caused by the annealing of defects in the surface layer of material as a result of temperature increase or deformation during blasting. It is well known that high purity aluminum can recrystallize at or below room temperature [28]. For example recrystallization of aluminum in dry sliding has been reported [29]. However, it has also been claimed that dynamic recrystallization does not occur in high purity aluminum because recovery processes are so rapid [30]. Kuo and Rigney [31] attributed the presence of grains free of dislocations in microstructure of high purity aluminum exposed to sliding test to dynamic or static recovery. In any case both recrystallization and recovery in the surface layer of the sample may lead to lower concentration of defects which is reflected in lower surface value of the S-parameter, Fig. 3. In [8] we suggested that similarity between the S-parameter depth distributions for copper samples exposed to blasting and exposed to sliding contact with a steel ball may be connected with the striking the sample surface with the ball during sliding.

4.2. Aluminum alloy

Improvement of the mechanical properties of the age-hardenable aluminum alloys is a consequence of the formation of precipitates. Final step of ageing of the aluminum alloy 6082 consists in creation of precipitates of the equilibrium β phase, Mg_2Si. The interfaces between precipitates and matrix may localize positrons e.g., incoherent Si precipitates [32]. Positrons in the raw samples of aluminum alloy may create localized states connected to the microstructure of precipitates or to defects induced by prior cold working e.g., forming a sheet.

For the aluminum alloy exposed to indentation with the load of 10 N the whole range of the W- and S-parameters changes is small. The slope of the straight line is associated with some error. Nevertheless, the slopes for the loads of 10 N and 20 N are equal within the experimental error. Similarly to the pure aluminum in the final range of depth the arrangement of the experimental point could suggest fitting of another straight line. The positron-trapping defects induced are similar

in both cases but they differ from the defects in pure aluminum alloys. The slope of the straight line for the blasted aluminum alloy has an even lower value. Therefore the dynamic blasting of aluminum alloy sample produces defect different from those induced by indentations, similarly as for the pure aluminum.

The positron annihilation spectrum reveals two components. The first one equal to (201 ± 1) ps exceeds definitely the bulk positron lifetime for aluminum. The value of the second lifetime component (305 ± 2) ps with intensity (18.0 ± 0.3)% can correspond to the annihilation of positrons trapped at clusters of three vacancies [26]. The mean positron lifetime $\bar{\tau}$ is equal to 220 ps. In the case of blasting of aluminum alloy the produced vacancy clusters are larger than in the pure aluminum but their concentration is smaller. Creation of larger vacancy clusters may be connected with the presence of the interfaces between the precipitates and bulk material.

In the case of copper [8] in which the vacancies do not anneal at room temperature the slope of the straight line in the W-S plot for the blasted sample was also lower than for the samples exposed to indentation. The positron lifetime measurement showed the lifetime component coming from single vacancies [33]. The average slope for the load of 5 N differed significantly from the slopes for the loads of 10 N and 20 N, for which the change of the slope was much smaller.

5. Conclusions

1. The kind of the positron trapping defects created by indentation in the pure aluminum as well as in the aluminum alloy does not depend on the load for the applied loads but differs from that caused by blasting. Generally defects produced in the aluminum alloy are different from those in the pure aluminum. In all cases the positron trapping defects do not change with the depth.

2. One can conclude from the measurement of the depth profile of the S-parameter that the von Mises criterion for yield defines the total depth range of open volume defects created during the indentation test in the pure aluminum. The detected S-parameter profile does not follow the principal stress distribution obtained within the elastic theory. Nevertheless the distinct drop of the S-parameter starts in the vicinity of the Hertz radius which could mark the border between the core and the plastic hemisphere.

3. The blasting process produced the depth distribution of the S-parameter which was described by the exponential decay function for both high purity aluminum and aluminum alloy. The exponential decay of the S-parameter is connected with the exponential decay of the defect concentration with the depth. The difference lies in the reduced surface value of the S-parameter for high purity aluminum. This indicates a lower concentration of positron-trapping defects in the vicinity of the surface as a result of recovery or recrystallization.

4. The PL measurements of the blasted pure aluminum indicate the presence of divacancies. In the case of the blasted aluminum alloy the vacancy clusters are larger and probably consists of three vacancies.

Acknowledgment

This work was supported by Committee for Scientific Research (Poland) under the grant No 2 P03B 008 24.

Appendix

The principal stresses in the rz plane are calculated using the equations [1]:

$$\sigma_{1,3} = \frac{\sigma_r + \sigma_z}{2} \pm \sqrt{\left(\frac{(\sigma_r - \sigma_z)}{2}\right)^2 + \tau_{rz}^2} \quad \text{(A1)}$$

$$\sigma_2 = \sigma_\theta \quad \text{(A2)}$$

$$\tau_{max} = \frac{1}{2}[\sigma_1 - \sigma_3] \quad \text{(A3)}$$

The above equations are obtained from the general formulae describing the stresses within the interior of the specimen given in cylindrical polar coordinates for a spherical indenter of radius r and the radius of contact area a (Equation 1).

Radial stress distribution is given by the equation:

$$\frac{\sigma_r}{p_m} = \frac{3}{2}\left\{\frac{1-2\nu}{3}\frac{a^2}{r^2}\left[1 - \left(\frac{z}{u^{1/2}}\right)^3\right] + \left(\frac{z}{u^{1/2}}\right)^3 \frac{a^2 u}{u^2 + a^2 z^2} + \frac{z}{u^{1/2}}\left[u\frac{1-\nu}{a^2+u} + (1+\nu)\frac{u^{1/2}}{a}\tan^{-1}\left(\frac{a}{u^{1/2}}\right) - 2\right]\right\}, \quad \text{(A4)}$$

where
$p_m = \frac{P}{\pi a^2}$—mean contact pressure, P is the load, ν is the Poison's ratio.

The hoop stress is calculated from the equation:

$$\frac{\sigma_\theta}{p_m} = -\frac{3}{2}\left\{\frac{1-2\nu}{3}\frac{a^2}{r^2}\left[1 - \left(\frac{z}{u^{1/2}}\right)^3\right] + \frac{z}{u^{1/2}}\left[2\nu + u\frac{1-\nu}{a^2+u} - (1+\nu)\frac{u^{1/2}}{a}\tan^{-1}\left(\frac{a}{u^{1/2}}\right)\right]\right\}. \quad \text{(A5)}$$

The axial stress:

$$\frac{\sigma_z}{p_m} = -\frac{3}{2}\left(\frac{z}{u^{1/2}}\right)^3\left(\frac{a^2 u}{u^2 + a^2 z^2}\right). \quad \text{(A6)}$$

The shear stress:

$$\frac{\tau_{rz}}{p_m} = -\frac{3}{2}\left(\frac{r z^2}{u^2 + a^2 z^2}\right)\left(\frac{a^2 u^{1/2}}{a^2 + u}\right), \quad \text{(A7)}$$

where:

$$u = \frac{1}{2}\{(r^2 + z^2 - a^2) + [(r^2 + z^2 - a^2)^2 + 4a^2z^2]^{1/2}\}. \quad \text{(A8)}$$

Along the z axis at $r = 0$ σ_r, σ_θ and σ_z are principal stresses. The two principal stresses are equal $\sigma_2 = \sigma_1$.

References

1. A. C. FISCHER-CRIPPS, "Introduction to Contact Mechanics" (Springer-Verlag, New York, Berlin, Heildelberg, 2000).
2. R. HILL, "The Mathematical Theory of Plasticity" (Claredon, Oxford, 1950).
3. A. C. FISHER-CRIPPS, *J. Mater. Sci*. **32** (1997) 727.
4. L. C. SMEDSKJAER, M. MANNINEN and M. J. FLUSS, *J. Phys. F: Met. Phys.* **10** (1980) 2237.
5. G. DLUBEK, O. BRÜMMER and E. HENSEL, *Phys. Stat. Sol.* (a) **34** (1976) 737.
6. B. SOMIESKI and R. KRAUSE-REHBERG, *Fatique Fract. Eng. Mater. Struct.* **24** (2001) 267.
7. S. HANSEN, U. HOLZWARTH, C. HUGENSCHMIDT, U. MÄNNIG, K.MAIER and T. WIDER, *Mater. Sci. Forum* **255–257** (1997) 536.
8. J. DRYZEK and E. DRYZEK, *Tribology Letters*, in press.
9. J. DRYZEK, E. DRYZEK, T. STEGEMANN and B. CLEFF, *Tribology Lett.* **3** (1997) 269.
10. J. DRYZEK, E. DRYZEK, F. BÖRNER and R. KRAUSE-REHBERG, *ibid.* **11** (2001) 29.
11. W. TRIFTSHÄUSER, *Phys. Rev.* B **12** (1975) 4634.
12. J. DRYZEK and E. DRYZEK, *Phys. Stat. Sol.* A **179** (2000) 337.
13. *Idem.*, *Nucleonika* **42** (1997) 87.
14. J. KANSY, *Nucl. Instr. Methods* A **374** (1996) 235.
15. R. L. CHAPLIN and H. M. SIMPSON, *Phys. Rev.* **163** (1967) 587.
16. T. FREDERIGHI, in "Lattice Defects in Quenched Metals," edited by R. M. J. Cotterill, M. Doyama, J. J. Jackson and M. Meshii (New York, NY, 1965).
17. K. PETERSEN, in "Positron Solid-State Physics," edited by W. Brandt (Amsterdam, New York, Oxford, 1983).
18. M. T. HUBER, *Ann. Phys*. **43** (1904) 61.
19. Information provided by Goodfellow.
20. K. L. JOHNSON, *J. Mech. Phys. Sol*. **18** (1970) 115.
21. H. HÄKKINEN, S. MÄKINEN and M. MANNINEM, *Europhys. Lett.* **9** (1989) 809.
22. P. HÄUTOJARVI, A. TAMMINEN and P. JAUHO, *Phys. Rev. Lett.* **24** (1970) 459.
23. H.-E. SCHAEFER, R. GUGELMEIER, R. SCHMOLZ and A. SEEGER, in "Microstructural Characterization of Materials by Non-Microscopical Techniques, Proceedings of the V Risø International Symposium of Metallurgy and Materials Science," edited by N. H. Andersen, M. Eldrup, N. Hansen, J. D. Jensen, T. Lefers, H. Lilholt, O. B. Pedersen and B. N. Singh (Risø National Laboratory, Denmark, 1984).
24. R. M. J. COTTERILL, K. PETERSEN, G. TRUMPY and J. TRÄFF, *J. Phys. F: Metal Phys.* **2** (1972) 459.
25. M. J. FLUSS, L. C. SMEDSKJAER, M. K. CHANSON, D. G. LEGNINI and R. W. SIEGEL, *Phys. Rev.* B **17** (1978) 3444.
26. M. J. PUSKA and R. M. NIEMINEN, *J. Phys. F: Met. Phys.* **13** (1983) 333.
27. CS. SZELES, ZS. KAJCSOS and A. VÉRTES, *Phys. Rev.* B **31** (1985) 1302.
28. F. HAESSNER and J. SCHMIDT, *Scr. Metal.* **22** (1988) 1917.
29. J. H. DAUTZENBERG, *Wear* **60** (1980) 401.
30. W. A. WONG, H. J. MCQUEEN and J. J. JONAS, *J. Inst. Met.* **93** (1967) 129.
31. S. M. KUO and D. A. RIGNEY, *Mater. Sci. Eng.* A **157** (1992) 131.
32. G. DLUBEK, O. BRÜMMER, R. KRAUSE, A. BARANOWSKI and B. ROZENFELD, *Phys. Stat. Sol.* (a) **78** (1983) 217.
33. J. DRYZEK, private communication.

Received 2 December 2002
and accepted 1 July 2003